Proceedings of the Korean Nuclear Society Spring Meeting
Gyeongju, Korea, May 2003

A Nucleate Boiling Limitation Model for the Prediction of Pool Boiling CHF

Heung June Chung [a], Hee Cheon No [b], Se Young Chun [a], Won Pil Baek [a]

[a] Korea Atomic Energy Research Institute
P.O. Box 105, Yusong, Daejon, 305-600, Korea

[b] Korea Advanced Institute of Science and Technology
373-1 Kusong-dong Yusong, Daejon 305-701, Korea

Abstract

A new nucleate boiling limitation model which can predict both the heat transfer in the nucleate boiling region and CHF is proposed for pool boiling on a horizontal surface. This model is developed based on the results of direct observations of the physical boiling phenomena. Verification of the performance of the prediction is accomplished by comparison with the existing experimental data. Verification results show that the present model incorporates the contact angle effect on CHF, and agrees well with experimental data.

1. Introduction

The accurate prediction of the boiling characteristic curve including critical heat flux (CHF) is essential for the design and safe operation of the high power density thermal systems such as boilers, heat exchangers, and nuclear reactors. Consequently, a plethora of empirical correlations and theoretical models on pool and flow boiling have been presented in these engineering fields. However, most current CHF models are mainly based on the postulation of the CHF phenomena without observation of the physical boiling phenomena. This is mainly due to the fact that the observation of the boiling phenomena near the heater surface is very difficult. Also, as several investigators suggested [1, 2], a realistic CHF model would be one that has a natural outcome of description of the high-heat flux nucleate boiling region in contrast to the traditional view of CHF as independent phenomena distinct from nucleate boiling.

Traditional CHF models may be classified into two categories: hydrodynamic instability model proposed by Zuber [3] and macrolayer dryout model presented by Haramura and Katto [4]. The main difference between the two models is in the location of the instability with respect to the heater. The hydrodynamic instability model by Zuber assumes that CHF is dictated by an instability in the vapor-liquid interface. Whereas, the macrolayer dryout model by Haramura and Katto postulates the onset of instability in the tiny vapor stems which intersperse the macrolayer immediately adjacent to the heater. One of the features of the hydrodynamic instability model is that it treats nucleate boiling and CHF as two independent entities. As Sadasivan et al. [1] pointed out that this is unrealistic because all variables affecting nucleate boiling influence transition boiling as well. Also, the macrolayer dryout model postulates that CHF occurs at the instant the macrolayer dries out during a period of vapor mushroom. This is not consistent with the experimental observation by Kirby and Westwater [5], Nishio et al. [6], and Chung and No [7], which show that at least for pool boiling, macrolayer never dries out at the CHF but dry spots or dry area occurs.

Liaw and Dhir [8] conducted pool boiling experiments for saturated water at atmospheric pressure on a vertical rectangular copper surface with several contact angles. They measured time and area-averaged void fraction, nucleate boiling heat fluxes including CHF. By using these experimental results, Dhir and Liaw [9] predicted CHF and transition boiling heat fluxes under the assumption of

the existence of the stationary vapor stems. This model seems to be successful in predicting CHF at a variety of contact angles. However, as Sadasivan et al. [1] indicated that this model is not realistic because vapor stems associated with individual nucleation sites are not distributed over the surface in a regular manner.

Very recently, Kolev [10], Zhao et al. [11] and Ha and No [2] presented theoretical models taking into consideration of the individual bubble behavior.

Kolev [10] considered the fluctuation frequency as a function of bubble departure frequency. This model shows a good agreement with experimental data. But, some empirical constants are introduced in the model to match the prediction to the experimental data.

Zhao et al. [11] formulated the microlayer model by considering the behaviors of individual bubbles beneath the vapor mushroom from the observations by Zhao et al [12] and Nishio et al. [6]. Even though their final prediction equation is somewhat complicated, the prediction results show fairly good agreement with the experimental data.

Ha and No [2] presented a dry spot model which can predict the CHF pool and flow boiling. They postulated that when nucleating bubbles in a cell exceed a critical number, the liquid supply into the cell stopped and dry spots occurred. Then, the dry spots coalesce with each other and CHF occurs. However, the dry spot formation mechanism is different from the experimental observation by Chung and No [7]. Therefore, the dry spot model requires to be modified to reflect the real dry spot formation mechanism.

As discussed above, a realistic CHF model would be one that incorporates the directly observed CHF mechanism rather than any postulations. Also, the model would be one that gives a natural outcome of description of the high-heat flux nucleate boiling region in contrast to the traditional view of CHF as independent phenomena distinct from nucleate boiling.

In the present study, based on the results of direct observations of the physical boiling phenomena near CHF, a new nucleate boiling limitation model which can predict the heat transfer in the nucleate boiling region including CHF is proposed for pool boiling on a horizontal surface. Verification of the performance of the prediction is accomplished by comparison with the existing experimental data.

2. Observation of CHF Mechanism

As described in the previous section, Chung and No [7] presented the directly observed CHF mechanism for pool boiling of R-113 on a horizontal surface. In their experiment, CHF was defined as the highest heat flux that the heater surface temperature maintained stable before temperature excursion commenced by a slight increase in the heat flux. At CHF, most of the heater surface becomes dry and the liquid-solid contact fraction decreases below 30 % and the wetted pattern is not a continuous plane type but maze-like curves. This wetted pattern is similar to the network pattern observed by Nishio et al. [6] and Oka et al. [13]. Also, at CHF, a large vapor film covers a great part of the heater surface, and intense nucleate boiling takes place around the edge of the large vapor film. Some nucleating bubbles in this locally-wetted region coalesce laterally and form another small vapor film. This small vapor film does not grow large, and a wetting region is formed repeatedly. This type of local nucleate boiling is similar to the observation by Galloway and Mudawar [14] for the flow boiling of FC-87.

A large vapor film, which covers a great part of the heater surface, collapses when its upper interface departs. After the large vapor film collapses, a short wetting occurs. If the surface is intermittently wetted, vigorous boiling occurs and a continuous vapor film resulting from the coalescence of vapor bubbles is reestablished. This experimental observation is similar to the observation of R-113 boiling by Nishio et al. [6], water boiling by Zhao et al. [12]. The vapor stems and the dryout of the macrolayer have not been observed. Instead of the vapor stems and dryout of the macrolayer, the local nucleate boiling occurs under the large vapor film and at the edge of it. From the above observations, it is noted that nucleate boiling takes place around the edge of the large vapor film and underneath the departing large vapor mass. This means that, even though the vapor film covers a large fraction of the heater surface, the local nucleate boiling in the wetted region plays a key role in determining the heater surface temperature not increasing further.

At CHF, the slight increase of heat flux causes the commencement of temperature excursion. This situation just after CHF is called CHF(+). At CHF(+), only a brief nucleate boiling occurs at the edge of a vapor film. However, the wetted region quickly becomes the dry region with a continuous vapor film and then nucleate boiling is limited by an agglomeration of nucleating bubbles. As a result of this limited nucleating boiling activity at the local wetted part of the heater surface, the heater surface temperature begins to increase further, resulting in a burnout. These observations are similar to the reduced boiling activity by Galloway and Mudawar [14] and Celata et al. [15]. Consequently, it can be concluded that CHF comes from the locally-limited nucleate boiling activity rather than any changes of hydrodynamic conditions.

3. A Nucleate Boiling Limitation Model

3.1. Concept of nucleate boiling fraction

As discussed in the previous section, the locally-limited nucleate boiling activity governs both CHF and the nucleate boiling heat transfer. In addition, Chung and No [7] experimentally investigated the dry spot formation mechanism and the role of the dry area under a large vapor mass. They found that the increased resident time of the large dry area in the local vapor film regime influences the heat transfer mechanism and, consequently, the slope of the boiling curve apparently changes. And, isolated dry spots or short periods of dry areas from isolated to coalesced bubble regimes hardly affect the boiling curve. One another important experimental observation by Chung and No [7] is that dry spots and bubbles occur simultaneously. This means that when a bubble nucleates and grows at a nucleation site, a dry spot is formed under the corresponding bubbles. Therefore, they should be considered as a synchronized identity rather than an independent one. Therefore, we can extract information about the number of bubbles from that of the dry spots.

Based on these experimental observations, the quantity of the heat transferred by all bubbles in the region that the coalescence effects is not strong and can be represented as $q_b \overline{N}$, where q_b is heat transferred by a single bubble site assuming each bubble site has a uniform heat duty and $\overline{N}$ is average density of the active nucleation sites. If we ignore the heat flux fractions due to single phase convection and film boiling, $q_b \overline{N}$ can be presumed as nucleate boiling heat flux, q_{NB}. The nucleate boiling heat flux curve can be estimated from the linear fitting of the nucleate boiling region as a function of the wall superheat as shown in Fig. 1. If there is no formation of the large dry area beyond the nucleate boiling region (Region II in boiling curve in Fig. 1), the heat flux increases along the curve q_{NB} with the surface superheat. However, as the large dry area occurs, the heat transfer deteriorates and the boiling curve deviates from the curve, q_{NB}. This is due to the decrease of the fraction of pure nucleate boiling without the coalescence of the bubbles. Therefore, if we can obtain the quantitative information on the pure nucleate boiling fraction in the coalesced boiling regime, we can evaluate the overall heat flux in region II under the assumptions that the heat flux fractions due to single phase convection and film boiling are negligible. Conclusively, the quantitative prediction of the nucleate boiling fraction in any boiling regime is essentially required in obtaining the overall heat flux.

Now, let us apply the concept of nucleate boiling fraction to the prediction of the R-113 pool boiling curve. To obtain the nucleate boiling fraction, first, the number of isolated bubbles without coalescence, N_b, in a given area, is counted from the behavior of dry spot experimentally observed by Chung and No [7]. And second, the active nucleation site density, N, is given using the Wang and Dhir's correlation [16] as follows:

$$N = 5 \times 10^{-27} (1 - \cos\phi) / d_c^6 . \tag{1}$$

where the cavity mouth diameter, d_c, is a function of the local superheating,

$$d_c = \frac{4\sigma T_{sat}}{\rho_g h_{fg} \Delta T}. \quad (2)$$

Then, we obtain the total number of bubbles in a given area A

$$N_A = N \text{ x } A. \quad (3)$$

For the present analysis, a contact angle of 14 degrees is used, because the experimental active nucleation site density agreed well with the case of 14 degrees as shown in Fig. 2. Then, the nucleate boiling fraction (*NBF*, Φ_{NB}) is defined as

$$\Phi_{NB} = N_b / N_A. \quad (4)$$

By using the above *NBF*, the overall heat flux from nucleate boiling to CHF can be represented as the following relation:

$$q = q_b \bar{N} \Phi_{NB} = q_{NB} \Phi_{NB}. \quad (5)$$

A comparison of the prediction using the concept of NBR with experimental data is shown in Fig. 3. As can be seen in this figure, the prediction has excellent agreement with the measured data from the nucleate boiling regime to the CHF. This result indicates that the nucleate boiling fraction should be one of the important quantities representing the nucleate boiling heat flux from the nucleate boiling regime to the CHF.

3.2. Basic assumptions

To simplify the modeling for both CHF and nucleate boiling heat flux, the followings are assumed:

(1) Time-averaged bubble diameter d_{av} is representative of the diameter of bubbles, since there are coexisting bubbles of all ages.

(2) The distribution of active nucleation sites obeys the Poisson distribution law as proposed by Gaertner [17]. Then, the probability that *NA* active sites will be found in a given area *A* can be calculated according to

$$P(n) = \frac{e^{-\overline{N_A}} \overline{N}_A^n}{n!}. \quad (6)$$

(3) As generally known, for the high-heat flux nucleate boiling up to CHF, the heat flux fractions due to pure natural convection and due to pure film boiling are much smaller than that due to pure nucleate boiling.

3.3. Proposed model

As discussed in the previous section, the nucleate boiling fraction (*NBF*) in a given boiling area defined as Eq. (4) is a key parameter for evaluating the heat flux contributing to nucleate boiling without coalescence.

Let us consider the arbitrarily selected area *A* as shown in Fig. 4. In this selected area, some isolated nucleating bubbles and coalesced bubbles coexist. As discussed in the previous section, isolated nucleating bubbles and coalesced bubbles correspond to the isolated dry spots and the coalesced dry areas, respectively. In these coexisting dry spots and areas, the probability of the

existence of isolated dry spots without coalescence is related to the *NBF*. As shown in Fig. 4, the dry area is a summation of the area occupied by totally isolated dry spots and the coalesced dry area, and the dry area fraction is defined as

$$\Gamma_{dry} = A_{dry} / A . \tag{7}$$

Then, if there are always some isolated dry spots and coalesced dry areas in area *A*, the dry area fraction contains the probabilities of isolated dry spots and dry areas, thus we can take it as

$$P(\Gamma_{dry,\,i}) \; + \; P(\Gamma_{dry,\,c}) = 1 , \tag{8}$$

and obtain

$$P(\Gamma_{dry,\,i}) \; = 1 \; - \; P(\Gamma_{dry,\,c}) , \tag{9}$$

where $P(\Gamma_{dry,i})$ is the probability of the dry area fraction occupied by isolated dry spots and $P(\Gamma_{dry,c})$ is the probability of the dry area fraction occupied by coalesced dry areas.

Based on the assumption that the distribution of active nucleation sites obeys the Poisson distribution, Hsu [18] studied many bubble populations of methanol and water on narrow heating strips and tabulated the percentage of merging bubbles as a function of heat flux and bubble size. By analyzing the experimental data, Hsu obtained the probability of coalescence between bubbles in one cell, *A*, in the following statistical relation:

$$P(Co) = 1 - e^{\overline{N}_A} (\overline{N}_A + 1) . \tag{10}$$

By utilizing Eqs. (9) and (10), we can obtain

$$P(\Gamma_{dry,\,i}) \; = 1 \; - \; \Gamma_{dry} \text{ x } P(Co) . \tag{11}$$

The Eq. (11) means the fraction of isolated bubbles without coalescence in a given area A. Then we can obtain the number of bubbles without coalescence contributing pure nucleate boiling

$$N_b = N \text{ x } A \text{ x } P(\Gamma_{dri,\,i}) \tag{12}$$

As described in Eq. (3), the number of bubbles in a given area A

$$N_A = N \text{ x } A . \tag{13}$$

Therefore, by utilizing Eqs. (12) and (13) we can obtain the nucleate boiling fraction, *NBF*, as follows:

$$\Phi_{NB} \; = \; N_b \; / N_A = 1 - \; \Gamma_{dry} \text{ x } P(Co) . \tag{14}$$

Subsequently, the heat flux contributing to the nucleate boiling is obtained as the following equation:

$$q = q_b \; \overline{N} \; \Phi_{NB} . \tag{15}$$

4. Prediction Results and Discussion

A comparison of the present model of Eq. (15) with experimental data was accomplished by using Liaw and Dhir's results [8]. Liaw and Dhir conducted pool boiling experiments for saturated water at atmospheric pressure on a vertical rectangular copper surface with several contact angles. As a first step for comparison, the reference dry area fraction for water, which is needed to calculate the number of bubbles in a given boiling area, is obtained from the regression of the experimental data by Chung and No [7]. Because, the contact angle in their experiment is the case of a somewhat lower range of contact angles (14 degrees). The regression equation as a function of wall superheat as:

$$\Gamma_{dry,\,ref} = 0.3631 - 0.0258\Delta T + 9.4019\text{x}10^{-4}\Delta T^2 \tag{16}$$

The experimental data for the dry area fraction given in most literatures covered the transition boiling region beyond the nucleating boiling region [19-21]. Therefore, there are little available data especially in the partial nucleate boiling regime. In the present study, to take into account the contact angle effect on the dry area fraction, the analytical results by Ha and No [22] were used. Based on the present experimental data as a reference contact angle and considering the effect of contact angle on the dry area fraction, the following incorporating equation was derived

$$\Gamma_{dry,\,\phi} = \Gamma_{dry,\,reference}\ \text{x}\ F(\phi)\,, \tag{17}$$

where

$$F(\phi) = 0.97 - 0.0038\phi + 3.68\text{x}10^{-4}\phi^2\,, \tag{18}$$

where ϕ is a contact angle as degree. The average density of active nucleation site is obtained by Wang and Dhir's correlation [16] given in Eqs. (1) and (2).

Figures 5 – 8 show the prediction results using water boiling data for several contact angles. We see from these figures that the prediction results agree well with the data in the region of nucleate boiling as well as CHF for all the contact angles. Also, the transition between before and after CHF on the boiling curve is very smooth. For all the cases, hydrodynamic theory by Zuber [3] does not show that the contact angle affects the CHF. This is due to the fact that the hydrodynamic theory is intended to predict only CHF and not to consider the nucleate boiling immediately preceding it. However, the present model well incorporates the contact angle effect on the CHF.

Based on the above discussion on the comparison with pool boiling data, we can infer the distinct features of the present model. First of all, during the development of the present nucleate boiling limitation model, the assumption that the overall heat flux is mainly due to the pure nucleate boiling in the high-heat flux nucleate boiling region is very appropriate. And, we can predict accurately both nucleate boiling heat transfer and CHF including the effect of contact angle with a single prediction equation. Also, the present model treats the CHF as a natural outcome at the end of nucleate boiling. This means that the present model is more realistic than any other model based on the postulations.

The present model was compared to the other water pool boiling data of Paul and Abdel-Khalik [23]. They conducted experiments on the pool boiling of saturated water at 1 atm with an electrically heated horizontal platinum wire. They measured active nucleation site density and bubble departure diameter up to 70 % of CHF. Mean number density of active nucleation sites per unit length and the average bubble departure diameter can be obtained from their results as follows:

$$\overline{N} = 1.207\text{x}10^{-3} q_{NB} + 15.74\,, \tag{19}$$

$$d_{\max} = 0.3874\text{x}10^{-9} q_{NB} + 1.108\text{x}10^{-3}\,. \tag{20}$$

The contact angle for this analysis is assumed as 38 degrees, and the measured CHF is 0.72×10^6 W/m^2 and the predicted value is 0.701×10^6 W/m^2 as shown in Fig. 7. The prediction error is about 2.7 %, and this shows better prediction accuracy than that of the dry spot model (8.7 %) by Ha and No [2].

In addition to the comparison with pool boiling data, we tried to investigate the extendibility of the present model to flow boiling. For investigation, the boiling parameters such as active nucleation site density and departure diameter need to be explicitly known. In the flow boiling experiments, Del Valle and Kenning [24] carried out subcooled flow boiling of water on a stainless steel plate, and explicitly presented the bubble diameter and active nucleation site density. They did not present the contact angle for the combination of water-stainless steel, therefore 69 degrees is assumed as the contact angle. They measured active nucleation site density and bubble departure diameter at heat fluxes of 70, 80, 90 and 95% of CHF at an inlet velocity of 1.7 m/s and 84 K inlet subcooling. The mean maximum bubble diameter was 0.4 mm ±5 % independent of heat flux, and active nucleation site density as a function of heat flux can be correlated as:

$$N = 2.30q + 10^6 . \tag{21}$$

The measured CHF was 4.92×10^6 W/m^2 and the predicted CHF by the present model is 4.91×10^6 W/m^2 as shown in Fig. 8. The discrepancy between the experimental CHF and predicted CHF is about 0.2%. The prediction accuracy of the present model is surprisingly satisfactory. From this verification, it can be noted that the application of the present model for the prediction of flow boiling CHF is possible under the conditions that the boiling parameters such as active nucleation site density and bubble diameter are known.

5. Conclusions and Recommendation

A new nucleate boiling limitation model, which can predict the heat transfer in the nucleate boiling region including CHF, was proposed for pool boiling on a horizontal surface. This model was developed based on the results of direct observations of the physical boiling phenomena. Verification of the performance of the prediction is accomplished by comparison with existing experimental data, and the following conclusions are derived:

1. The present nucleate boiling limitation model predicts both the heat transfer in a fully developed nucleate boiling region and the CHF for pool boiling with fairly good accuracy. This proposed model also incorporates the contact angle effect on the CHF.
2. The present model treats the CHF as a natural outcome of the end of nucleate boiling. This means that the present model is more realistic than any other proposed model based on the postulations.
3. Comparing the prediction results with flow boiling experimental data shows an excellent agreement with flow boiling CHF data. This means that, if the boiling parameters such as active nucleation site density and bubble diameter are explicitly known, the application of the present model for the prediction of flow boiling CHF is reasonably possible.
4. A single prediction model was applied to quite different boiling conditions, pool and flow boiling, without any correction. It strongly supports that the basic CHF mechanism is not very different even though the boiling conditions are very different.
5. To verify the present model, experimental data such as active nucleation site density, and bubble diameter, and dry area fraction were used. Further work on them, especially for flow boiling, can contribute to the improvement of the present model.

References

[1] P. Sadasivan, C. Unal, R. Nelson, Perspective: issues in CHF modeling - the need for new experiments, ASME Journal of Heat Transfer 117 (1995) 558-567.

[2] S. J. Ha, H. C. No, A dry-spot model of critical heat flux in pool and forced convection boiling,

International Journal of Heat and Mass Transfer 41 (2) (1998) 303-311.
[3] N. Zuber, Stability of boiling heat transfer, ASME Journal of Heat Transfer 80 (1958) 711-720.
[4] Y. Haramura, Y. Katto, A new hydrodynamic model of critical heat flux, applicable widely to boiling to both pool and forced convection boiling on submerged bodies in saturated liquid, International Journal of Heat and Mass Transfer 26 (1983) 389-399.
[5] D. B. Kirby, J. W. Westwater, Bubble and vapor behavior on a heated horizontal plate during pool boiling near burnout, Chemical Engineering Progress Symposium Series, 61(57), 1965, pp. 238-248.
[6] S. Nishio, T. Gotoh, N. Nagai, Observation of boiling structures in high heat-flux boiling, International Journal of Heat and Mass Transfer 41 (1998) 3191-3201.
[7] H. J. Chung, H. C. No, Simultaneous visualization of dry spots and bubbles for pool boiling of R-113 on a horizontal heater, International Journal of Heat and Mass Transfer 46 (2003) 2239-2251.
[8] S. P. Liaw, V. K. Dhir, Void fraction measurements during saturated pool boiling of water on partially wetted vertical surfaces, ASME Journal of Heat Transfer 111 (1989) 731-738.
[9] V.K. Dhir, S. P. Liaw, Framework for a unified model for nucleate and transition pool boiling, ASME Journal of Heat Transfer 111 (1989) 739-746.
[10] N. I. Kolev, How accurately can we predict nucleate boiling ?, Experimental Thermal and Fluid Science, 10 (1995) 370-378.
[11] Y. H. Zaho et al., Unified theoretical prediction of fully developed nucleate boiling and critical heat flux based on a dynamic microlayer model, International Journal of Heat and Mass Transfer 45 (2002) 3189-3197.
[12] Y. H. Zaho et al., Boiling bubble behavior and heat transfer characteristics on a horizontal Pt-wire within a narrow space, Proceedings of heat transfer seminar of JSME, Okinawa, Japan, 1994, pp. 238-241.
[13] T. Oka et al., Pool boiling of n-pentane, CFC-113, and water under reduced gravity: parabolic flight experiments with a transparent heater, ASME Journal of Heat Transfer 117 (1995) 408-417.
[14] J. E. Galloway, I. Mudawar, CHF mechanism in flow boiling from a short heated wall-I. Examination of near-wall conditions with the aid of photomicrography and high-speed video imaging, International Journal of Heat and Mass Transfer 30 (10) (1993) 2511-2526.
[15] G. P. Celata et al., Visual investigation of high heat flux burnout in subcooled flow boiling of water, Third International Conference on Multiphase Flow, ICMF'98, Lyon, France, 1998.
[16] C. H. Wang and V. K. Dhir, Effect of surface wettability on active nucleation site density during pool boiling of water on a vertical surface, ASME Journal of Heat Transfer 115 (1993) 659-669.
[17] R. F. Gaertner, Distribution of active sites in the nucleate boiling of liquids, Chemical Engineering Progress Symposium Series, 59(41), 1963, pp. 52-61.
[18] Y. Y. Hsu, R. W. Graham, Transport Processes in Boiling and Two-Phase Systems, Mcgraw-Hill, New York, 1976, pp. 39-49.
[19] A. A. Alem Rajabi, R. H. S. Winterton, Liquid-solid contact in steady-state transition pool boiling, International Journal of Heat and Fluid Flow 9(2) (1988) 215-219.
[20] D. S. Dhuga, R. H. S. Winterton, Measurements of surface contact in transition, International Journal of Heat and Mass Transfer 28(10) (1985) 1869-1880.
[21] H. S. Ragheb, S. C. Cheng, Surface wetted area during transition boiling in forced convective flow, ASME Journal of Heat Transfer 101 (1979) 381-383.
[22] S. J. Ha, H. C. No, A dry-spot model for transition boiling heat transfer in pool boiling, International Journal of Heat and Mass Transfer 41 (1998) 3771-3779.
[23] D. D. Paul, S. I. Adel-Khalik, A statistical analysis of saturated nucleate boiling along a heated wire. International Journal of Heat and Mass Transfer 26(4) (1983) 509-519.
[24] Victor H. Del Valle M., D. B. R. Kenning, Subcooled flow boiling at high heat flux, International Journal of Heat and Mass Transfer 28(10) (1985) 1907-1920.

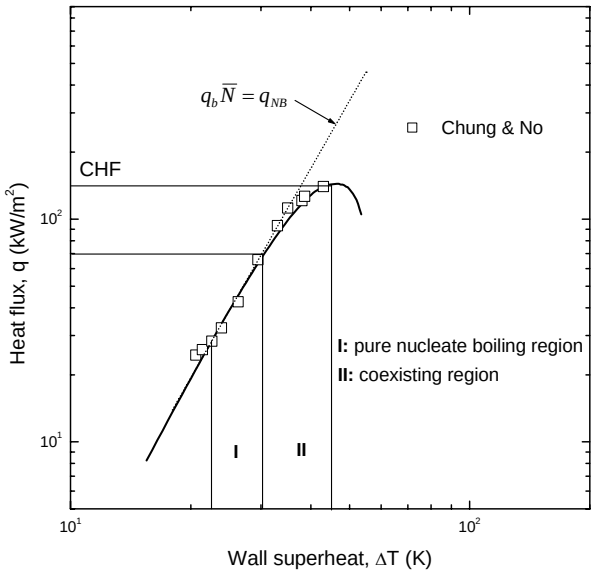

Fig. 1. Typical boiling curve.

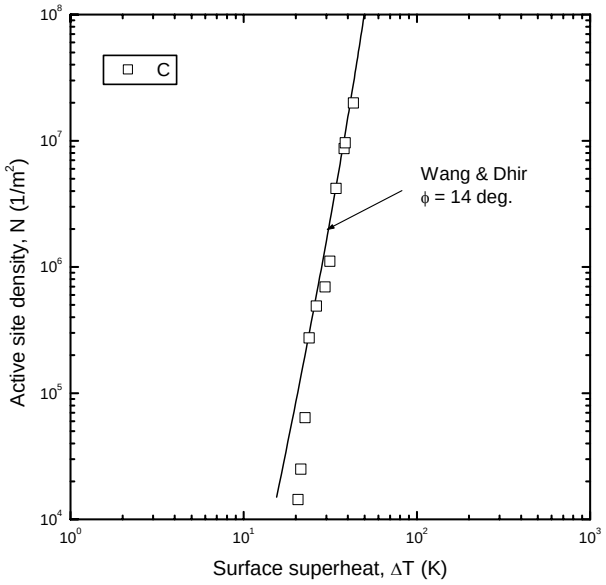

Fig. 2. Active site density for pool boiling of R-113.

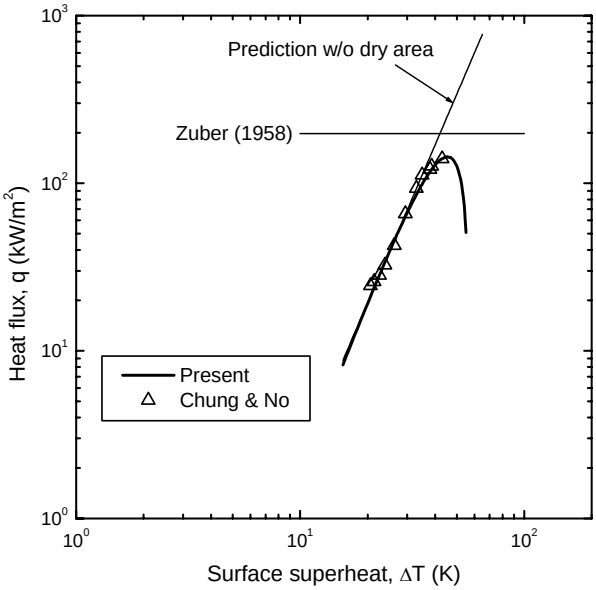

Fig. 3. Comparison of prediction with R-113 pool boiling data using concept of nucleate boiling fraction.

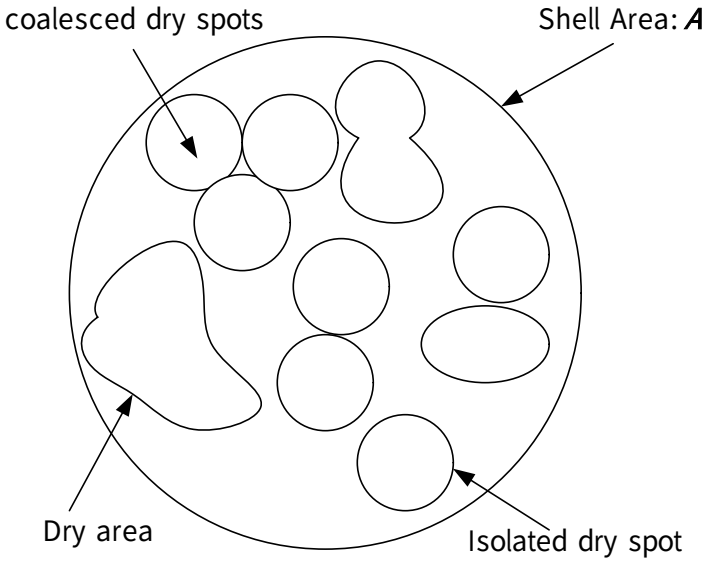

Fig. 4. Configuration of the conceptual dry area.

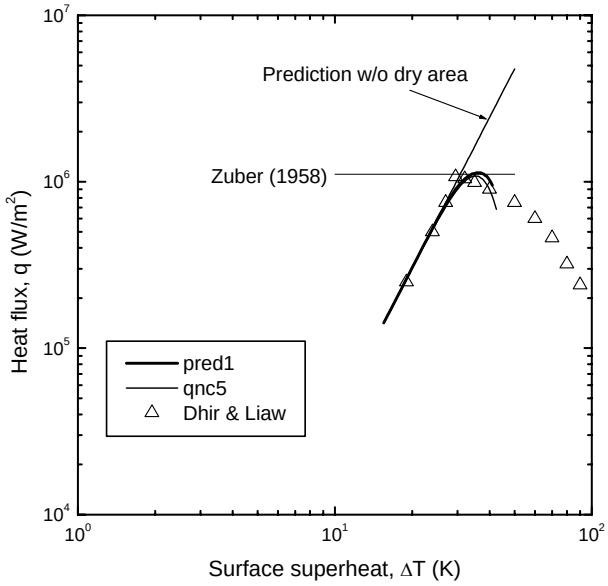

Fig. 5. Comparison of prediction with experimental data for contact angle of 14 degrees.

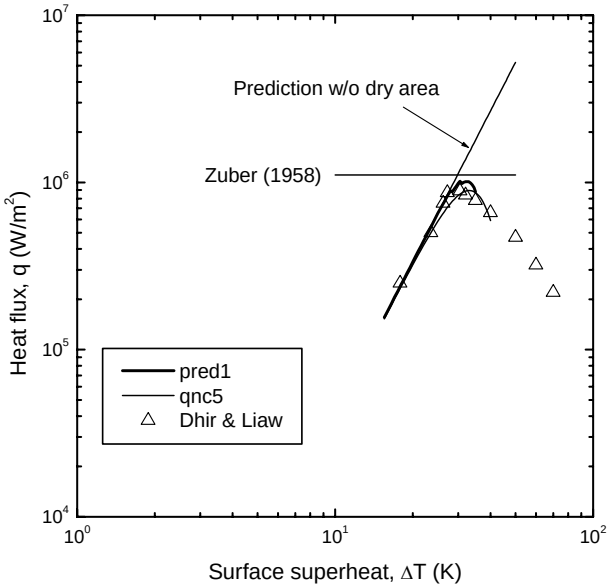

Fig. 6. Comparison of prediction with experimental data for contact angle of 27 degrees.

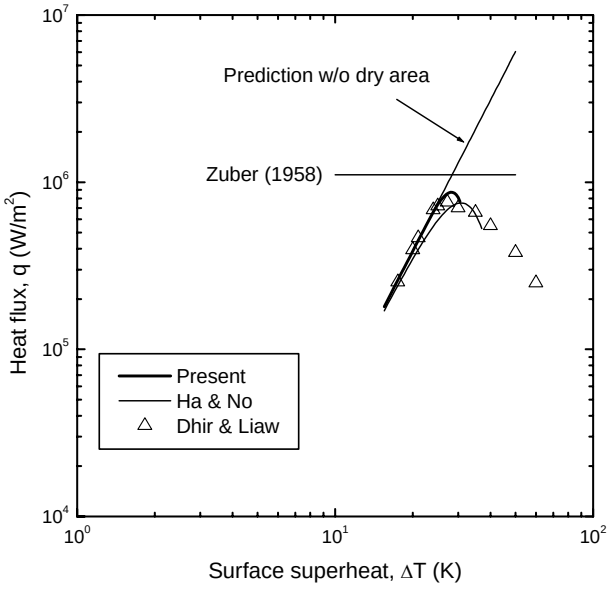

Fig. 7. Comparison of prediction with experimental data for contact angle of 38 degrees.

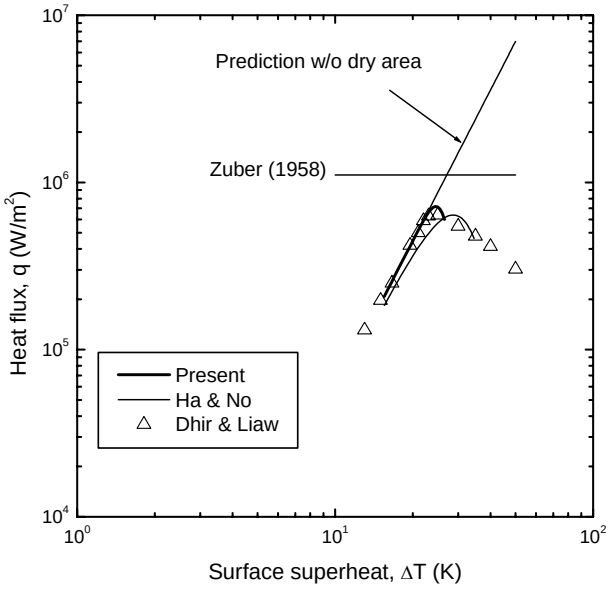

Fig. 8. Comparison of prediction with experimental data for contact angle of 69 degrees.

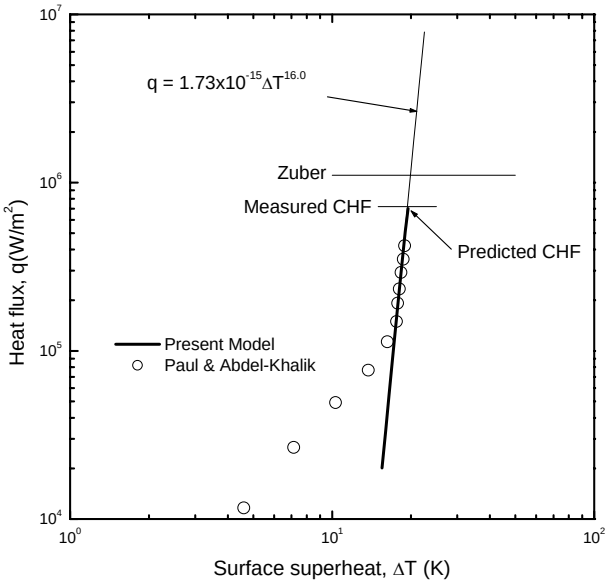

Fig. 9. Comparison of predictions with data for horizontal wire.

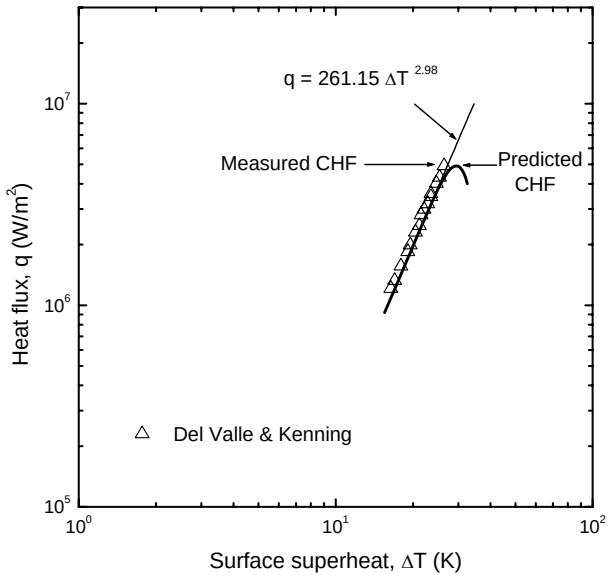

Fig. 10. Comparison of predictions with data for subcooled flow boiling.